

# Simulation of fracture and fatigue damage in stainless steel 304 using a cohesive zone model

Huan Li, Huang Yuan\*

Department of Mechanical Engineering, University of Wuppertal, Germany.

\* Corresponding author: h.yuan@uni-wuppertal.de

---

**Abstract** In the present paper a cohesive zone model coupled with monotonic and cyclic damage mechanisms for simulating elastic-plastic fracture and fatigue crack growth is introduced and applied for investigating failure processes in compact tension specimens. Fracture and fatigue crack tests are conducted on the compact tension C(T) specimen made of stainless steel 304 to study crack growth behavior under fracture and low cycle fatigue loading condition associated with severe elastic-plastic deformations. A good agreement between the prediction and the experimental result is obtained from the present simulations. It confirms that the suggested cohesive model in conjugation with the nonlinear damage evolution equations is applicable for describing the material degradation behavior of stainless steel 304 under both monotonic and cyclic loading with large plastic deformations.

**Keywords** Cohesive model, damage evolution, low cycle fatigue, elasto-plastic growth, crack growth rate

---

## 1. Introduction

Fatigue crack in industrial components are often subjected to heavy cyclic loading, and it is important to predict the fatigue crack growth behavior under higher stress fields. In low cycle metal fatigue problems, e.g. under loading conditions with maximum stresses beyond yield stress, specimens fail in small numbers of loading cycles.

Comparing with Paris' law, Walker model and Forman model or any other kinds of stress intensity factor based models, the cohesive model is more advantageous and gives the possibility to analyze the fatigue propagation behavior under severe plastic loading conditions, since the characterization of the cohesive zone model is generally applicable for inelastic materials [1-7]. Furthermore, it becomes possible to describe crack nucleation and propagation uniformly by the cohesive model.

Originally, the cohesive zone model was introduced to describe the fracture process zone ahead of the crack-tip by Dugdale [8] and Barenblatt [9]. In the last twenty years, the cohesive modeling has been applied in simulating monotonic fracture process for diverse materials and has also been verified by experimental results [10-13]. For the fatigue failure analysis, the loading history dependent development of material degradation has to be taken into account under cyclic loading. Establishing a physical solid cohesive model for finite fatigue life is under intensive investigation in many research groups worldwide [2, 3, 14-17].

In the present study, the fatigue crack propagation experiments have been conducted using compact tension C(T) of type 304 stainless steel associated with large plastic deformations. A cohesive model coupled with damage for prediction of fracture and fatigue behavior is introduced for elastic-plastic crack propagation associated with both normal and shear displacements of the crack surface. Both rupture damage and cyclic damage accumulation are considered in the damage evolution equations. The numerical results agree with experimental data and reproduce the high

fatigue crack propagation rate. The present analysis is limited to a two-dimensional configuration by the plane strain assumption.

## 2. Experimental arrangement

### 2.1. Material and specimens

The material used in the present investigation comes with 304 austenitic stainless steel cylindrical bars with a 200mm diameter. The mechanical properties were obtained through tensile test performed on cylindrical specimen of 6mm diameter and about 70mm gauge length. The C(T) specimens were fabricated following the ASTM E399. The dimensions of C(T) specimen are illustrated in Figure 1(a). The material curves are shown in Figure 1(b).

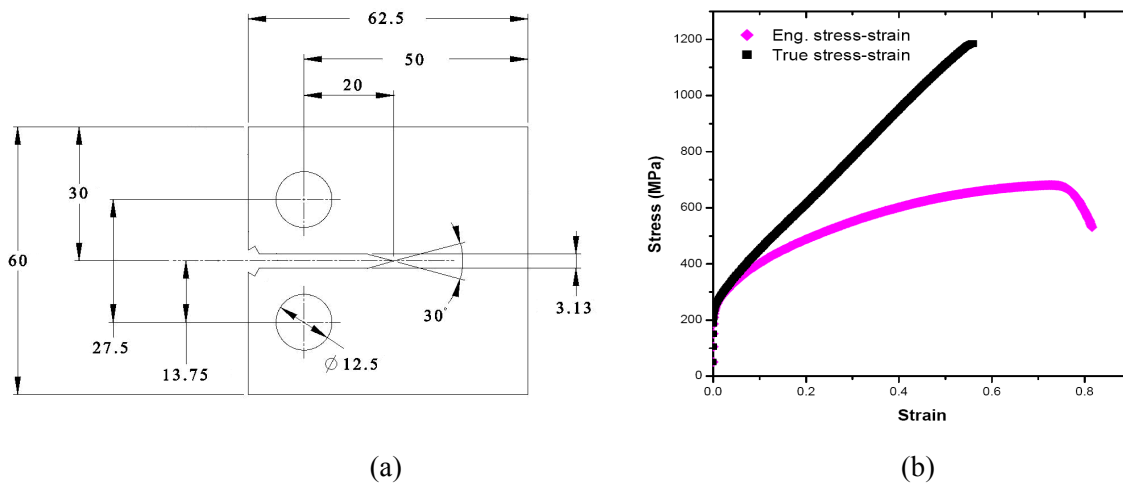


Figure 1. (a) Dimensions of C(T) specimen, the thickness is 12.5mm. (b) Engineering and true stress-strain curves for the stainless 304 steel.

### 2.2. Experimental apparatus and conditions

The configuration of clevis used for C(T) specimen is based on ASTM E647. All fatigue pre-cracks of the specimens were generated under mode I loading using high frequency testing machine at a loading frequency of approx. 90 Hz. The fracture test was conducted to determine the plane strain fracture toughness of the stainless steel 304. Fatigue loading during the crack growth process was carried out in a MTS servo-hydraulic testing machine.



Figure 2. (a) The compliance method and (b) beachmarks on the fracture surface for CT specimen.

The tests were performed in air at room temperature with sine waveform at a frequency of 8 Hz. The fatigue crack growth rate was measured by using the compliance method and also creating beachmark to record the crack front as displayed in Figure 2.

### 3. Cohesive zone model

#### 3.1. Kinematics and constitutive relation under quasi-static and cyclic loading

Taking the principle of virtual work of the boundary value problem into account, the weak form of the equilibrium equation without body forces can be written as

$$\int_V \boldsymbol{\sigma} : \delta \boldsymbol{\varepsilon} dV + \int_S \mathbf{T} \cdot \delta \Delta dS = \int_{\partial V} \mathbf{T}' \cdot \delta \mathbf{u} ds \quad (1)$$

with  $\boldsymbol{\sigma}$  as the Cauchy stress tensor,  $\mathbf{T}'$  denotes the external traction vector and  $\langle \delta \boldsymbol{\varepsilon}, \delta \Delta, \delta \mathbf{u} \rangle$  are the admissible displacement fields. The cohesive traction  $\mathbf{T}$  is taken to have the following form,

$$\mathbf{T} = T_s \mathbf{s} + T_n \mathbf{n} = \frac{T}{\Delta} (\xi^2 \Delta_s \mathbf{s} + \Delta_n \mathbf{n}), \quad (2)$$

where  $T_s$  and  $T_n$  are the cohesive traction components in shear and normal direction, respectively. Following the Ortiz et al. [1] and Ural et al. [17], the effective displacement jump  $\Delta$  is a scalar parameter defined as

$$\Delta = \sqrt{\xi^2 \Delta_s^2 + \Delta_n^2}, \quad (3)$$

where  $\Delta_s = |\Delta_s|$  and  $\Delta_n$  are the displacement jumps in shear and normal directions and  $\xi$  weights the shear displacement jump over normal one.  $T$  is a scalar effective traction relates to the effective displacement jump  $\Delta$  in the process zone where a crack may arise. The formulation of  $T$  used in the present study refers to a coupled damage model defined as

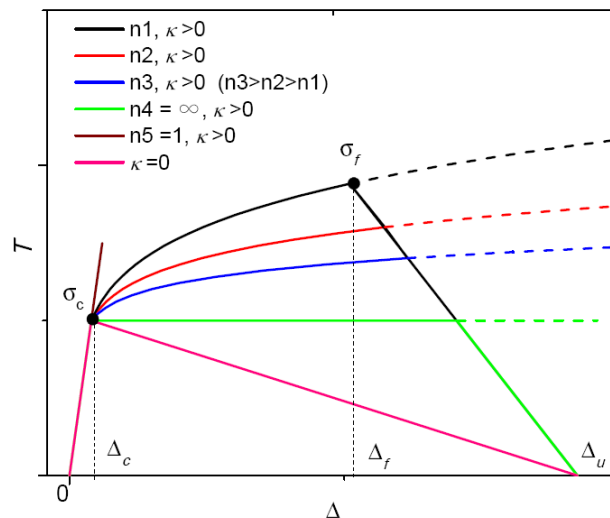


Figure 3. Illustration of the cohesive zone model under monotonic loading.

$$\Delta = \begin{cases} \frac{T}{\sigma_c} \Delta_c + \kappa \left( \frac{T}{\sigma_c} \right)^n & 0 \leq \Delta \leq \Delta_f \\ -\frac{T}{\sigma_f} (\Delta_u - \Delta_f) + \Delta_u & \Delta_f < \Delta \leq \Delta_u \end{cases}, \quad (4)$$

where  $\Delta_c$  is the onset of the displacement jump associated with initiation of the cohesive zone hardening,  $\sigma_c$  refers to the initial cohesive strength of the process zone corresponding to  $\Delta_c$  and  $\Delta_u$  is the final displacement jump which mirrors the complete loss of stress carrying capacity when the traction equals to zero.  $\kappa$  is a parameter which has the same unit as the displacement jump and  $n$  is the hardening exponent.  $\Delta_f$  is the value of displacement jump after which the initiation of damage begins and the corresponding cohesive strength is  $\sigma_f$ , the effects of these parameters are shown in Figure 3. For the application of Eq. (4), the inequality must be satisfied that

$$T \leq C(D) = \sigma_f(1 - D), \quad (5)$$

where  $D$  is a scalar variable representing the overall damage in materials and  $C$  is identified with the cohesion as the function of the damage. The monotonic cohesive law is insufficient and the cyclic damage should be taken into account in the constitutive description. Should the cohesive model be applied for both fracture and fatigue crack growth, the material damage depends on both monotonic loading and loading cycles, i.e.

$$\frac{dD}{dt} = \dot{D} = \dot{D}_s + \dot{D}_c \quad (6)$$

with  $D_s$  for damage under monotonic loading and  $D_c$  for damage under cyclic loading. Obviously, both damage variables have to be expressed in evolution equations.

Under the monotonic loading condition, Eq. (4) denotes inelastic behavior of the material in the cohesive zone and Eq. (5) implies that the degradation of the material strength for  $\Delta < \Delta_f$ . For  $\Delta > \Delta_f$ , the damage grows and assumes to be expressed in a linear function of the displacement increment [17],

$$D_s = \frac{\Delta - \Delta_f}{\Delta_u - \Delta_f} \quad (7)$$

under monotonic loading condition.

For fatigue, the material should be damaged even under the cohesive strength,  $\sigma_f$ . The damage evolution equation proposed by Ural et al. [17] is used to characterize fatigue process reads

$$\dot{D}_c = \begin{cases} \alpha D_c (T - \beta C) \dot{\Delta} & T - \beta C > 0, \dot{\Delta} > 0 \\ \gamma D_c (T - \beta C) \dot{\Delta} & T - \beta C < 0, \dot{\Delta} < 0 \\ 0 & (T - \beta C) \dot{\Delta} < 0 \\ \dot{\lambda} & T = C, \dot{\Delta} > 0 \end{cases}, \quad (8)$$

where  $\alpha$  and  $\gamma$  are two difference material constants used to conduct the damage accumulation during the reloading and unloading under the given conditions, respectively. The parameter  $\beta$  is adopted to denote the fatigue threshold in conjunction with the current cohesion  $C$ . The rate form of  $\lambda$  is a free variable is defined to represent the damage growth rate at a random stress state associated with the second equation of Eq. (4).

Following the suggestion in [17], the unloading and reloading paths of the present study can be

described in the incremental form as

$$\dot{T} = F(D)\dot{\Delta} \quad \text{with} \quad F(D) = \frac{\sigma_f(1-D)}{D(\Delta_u - \Delta_f) + q\Delta_c} \quad \text{and} \quad q = \frac{\sigma_f}{\sigma_c}. \quad (9)$$

The equation above indicates that the unloading/reloading stiffness the cohesive zone,  $F(D)$ , varies with  $D$  from  $\sigma_c/\Delta_c$  for no damage ( $D=0$ ) to zero for  $D=1$ .

The total damage in terms of a loading history should be the sum of the monotonic damage and cyclic damage

$$\dot{D} = \dot{D}_s + \dot{D}_c = \frac{\dot{\Delta}}{\Delta_u - \Delta_f} + \dot{D}_c \quad (10)$$

### 3.2. Implementation of cohesive element into ABAQUS

The commercial software ABAQUS[18] allows the user to define a new element conveniently, via the interface UEL. The formulation of the cohesive element is referred to the ABAQUS theoretical manual. We have to provide the cohesive element stiffness, the residual nodal force vector and derive the cohesive traction and displacement jump according to the cohesive law. These variables are needed to calculate the virtual work generated by the cohesive zone such that the internal work equals to the external virtual work for every kinematically admissible displacement field in accordance with Eq. (1). As illustrated in Figure 4, a four node cohesive element is defined in two dimensional  $x$ - $y$  coordinates. The nodal displacement vector corresponding to 4 nodes is defined by

$$\mathbf{u} = [u_i, v_i]^T \quad i = 1, 2, 3, 4 \quad (11)$$

with  $u$  and  $v$  as nodal displacements in  $x$  and  $y$  direction, respectively. Then the local displacement jump vectors  $\Delta$  are written using the shape functions and the nodal displacement as

$$\Delta = \begin{bmatrix} \Delta_s \\ \Delta_n \end{bmatrix} = \boldsymbol{\alpha} \mathbf{B} \mathbf{u} \quad (12)$$

with  $\mathbf{B}$  as the matrix about the shape functions,

$$\mathbf{B} = \begin{bmatrix} -N_1 & 0 & -N_2 & 0 & N_2 & 0 & N_1 & 0 \\ 0 & -N_1 & 0 & -N_2 & 0 & -N_2 & 0 & N_1 \end{bmatrix}, \quad (13)$$

where  $N_1=(1-s)/2$  and  $N_2=(1+s)/2$  are linear interpolation functions in the intrinsic coordinate system and  $\boldsymbol{\alpha}$  is the rotation matrix denoted by

$$\boldsymbol{\alpha} = \begin{bmatrix} \cos \theta & \sin \theta \\ -\sin \theta & \cos \theta \end{bmatrix}. \quad (14)$$

The cohesive element stiffness matrix and the traction force term are given by

$$\begin{aligned} \mathbf{K}^e &= \int_e \mathbf{B}^T \mathbf{D} \mathbf{B} dA = \frac{l_e}{2} \int_{-1}^1 \mathbf{B}^T \mathbf{D} \mathbf{B} ds, \\ \mathbf{T}^e &= \int_e \mathbf{B}^T \mathbf{T} dA = \frac{l_e}{2} \int_{-1}^1 \mathbf{B}^T \mathbf{T} ds, \end{aligned} \quad (15)$$

where  $l_e$  is the length of the element,  $\mathbf{T}$  is the traction vector based on the Eq. (2) and  $\mathbf{D}$  is the

material Jacobian matrix denoted as

$$\mathbf{D} = \begin{bmatrix} \frac{dT_s}{d\Delta_s} & \frac{dT_s}{d\Delta_n} \\ \frac{dT_n}{d\Delta_s} & \frac{dT_n}{d\Delta_n} \end{bmatrix}. \quad (16)$$

During the implementation, the matrices of Eq. (15) should be transformed to  $x$ - $y$  coordinates according to Eq. (14).

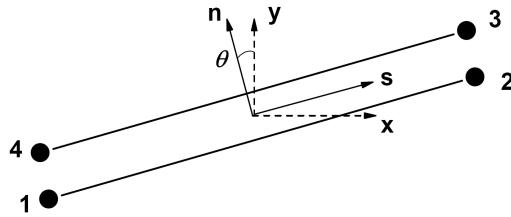


Figure 4. Illustration of a cohesive element

## 4. Results and discussion

### 4.1. Crack growth under monotonic loading

C(T) specimens were tested to determine cohesive parameters under monotonic loading. The load-displacement curve was recorded in the experiment. In computations the finite element mesh of the potential damage zone ahead of the crack tip is refined and the minimal element size is about 0.4mm. In the process of numerical simulation, cohesive elements are placed at the symmetric line of the mesh with zero thickness. The rest of region is occupied by the conventional four nodal elements under the plane strain assumption. The initial crack length is around 29mm. The stainless steel is described by the  $J_2$  plasticity for simplicity.

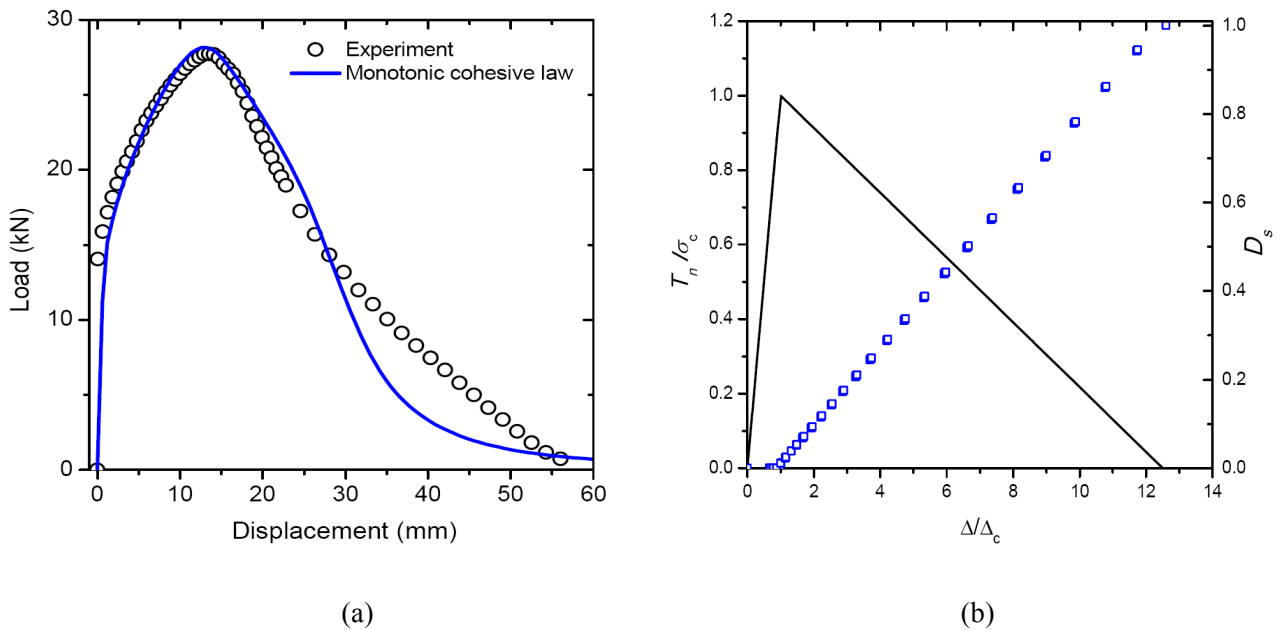


Figure 5. Computational prediction of monotonic crack growth in a C(T) specimen. (a) Comparison between the simulation and the test result. (b) Cohesive response of a ruptured element during the crack propagation.

As mentioned in the previous sections, Eq. (4) shows the bilinear behavior if  $\kappa=0$  under the monotonic loading and the initial cohesive strength of  $\sigma_c=\sigma_f=1100\text{MPa}$  associated with  $\Delta_c=\Delta_f=0.2\text{mm}$ . Computational simulation based on the cohesive zone model according to Eq. (4) is shown in Figure 5(a) for monotonic fracture. It confirms that the final displacement jump  $\Delta_u=2.5\text{mm}$  gives a reasonable prediction in comparing with the experiment. This kind of the cohesive law is popular in simulation of quasi-brittle material failure. Figure 5(b) illustrates the cohesive response of a ruptured element along crack path, the static damage evolution of the element can be seen additionally and this result should be imagined according to Eq. (7) or Eq. (10).

#### 4.2. Crack growth under cyclic loading

The crack growth under cyclic loading case is conducted within elasto-plastic region in this section. Considering the cyclic damage equation as mentioned in Eq. (8), the damage accumulation depends on the current cohesive traction and the increment of the displacement jump corresponding to the loading history. We use the concept of the loading cycles to capture the evolution of damage and predict the fatigue life. By recording the crack growth length,  $\Delta a$ , the fatigue crack growth rate can be determined by  $\Delta a/\Delta N$ . Since the global loading behavior of the C(T) specimen is represented by the amplitude of the stress intensity factor,  $\Delta K$ , the numerical simulation by using the cohesive element can be verified through the experimental  $da/dN$  vs.  $\Delta K$  curve.

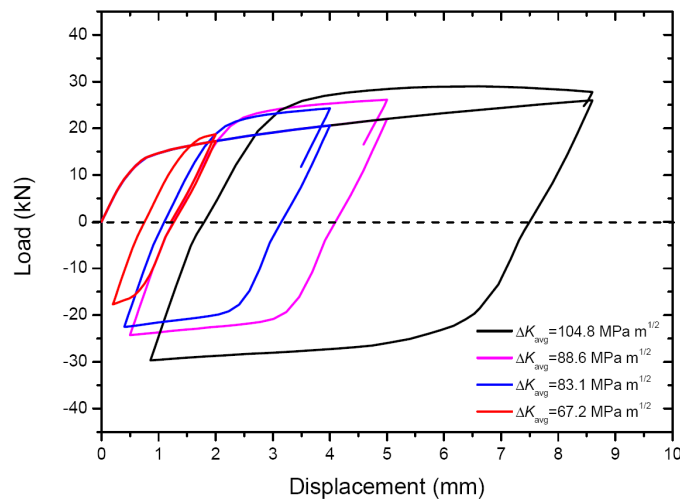


Figure 6. Four loading amplitudes for the CT specimen as a function of load line displacement.

As shown in Figure 6, four different loading amplitudes were performed under the displacement control at the loading ratio  $R=0.1$ . Because the stainless steel 304 is a cyclic instable material which associates the stress variation as a function of loading cycles, the average stress amplitude  $\Delta K_{\text{avg}}$  is used to express the loading level during the crack growth process. The specimen dimensions and mesh configurations for the fatigue simulation are the same as those for the fracture test. The material parameters for the damage evolution are  $\alpha=0.00053$ ,  $\beta=0.15$  and  $\gamma=0.0$  combined with the monotonic cohesive law which has been determined from the fracture simulation. The damage growth process in an element ahead of the crack-tip is displayed in Figures 7, 8 and 9 under the conditions with  $\Delta K_{\text{avg}}=83.1\text{MPa m}^{1/2}$  and  $\Delta K_{\text{avg}}=104.8\text{MPa m}^{1/2}$ , respectively. In the figures, the traction and displacement jump are non-dimensionalized by  $\sigma_c$  and  $\Delta_c$ , respectively. The negative displacement jump associated the compression of the crack surface is constrained by introducing a

penalty equation for contact. Comparing the amplitudes, the higher loading level results in a faster material degradation (Figure 7) and so shorter fatigue life (Figure 8). Actually,  $\Delta K_{avg}=104.8 \text{ MPa m}^{1/2}$  asymptotically approaches the plain strain toughness  $K_c$  of  $133 \text{ MPa m}^{1/2}$  at the loading ratio  $R=0.1$ , larger amount of damage accumulation is coincident with that caused by the fracture loading. In Figure 8, the traction against the loading segment (half cycle) is illustrated in both loading and unloading path, no damage growth is assumed in the unloading path including the compression in terms of Eq. (8), as shown in Figure 9. In order to verify the simulation results, the popular crack growth law proposed by Erdogan et al. [19] is used to consider all ranges of cyclic crack growth which is given by

$$\frac{da}{dN} = \frac{C(\Delta K - \Delta K_{th})^n}{(1-R)K_c - \Delta K}, \quad (17)$$

where the fracture toughness of  $K_c=133 \text{ MPa m}^{1/2}$ , the threshold value of  $\Delta K_{th}$  is  $7.5 \text{ MPa m}^{1/2}$  and material constants  $C=10^{-5.578}$  and  $n=2.697$  for correlating the experimental data. The computational result together with the experiment are compared in Figure 10, the prediction gives a better agreement with the test, especially in the region III of fatigue crack growth.

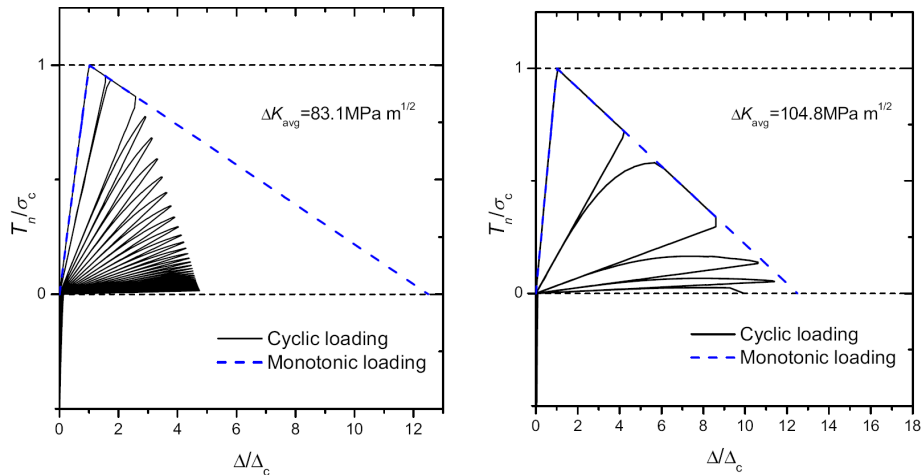


Figure 7. The traction vs. displacement jump curves in a cohesive element for  $\Delta K_{avg}=83.1 \text{ MPa m}^{1/2}$  and  $\Delta K_{avg}=104.8 \text{ MPa m}^{1/2}$ .

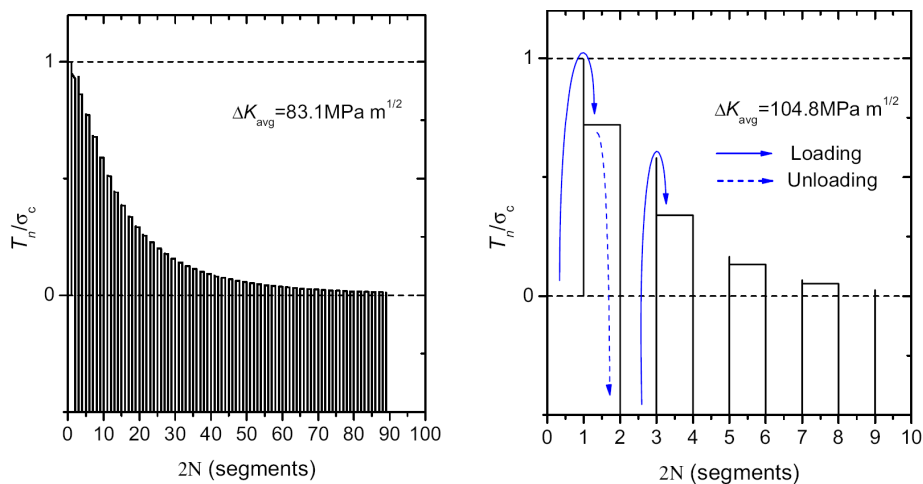


Figure 8. The traction vs. loading segments curves for  $\Delta K_{avg}=83.1 \text{ MPa m}^{1/2}$  and  $\Delta K_{avg}=104.8 \text{ MPa m}^{1/2}$ .

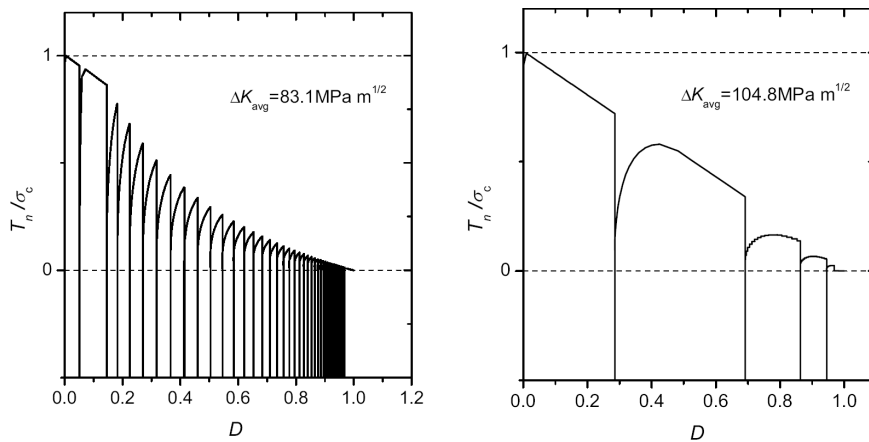


Figure 9. The traction vs. damage evolution curves for  $\Delta K_{avg}=83.1\text{MPa m}^{1/2}$  and  $\Delta K_{avg}=104.8\text{MPa m}^{1/2}$ .

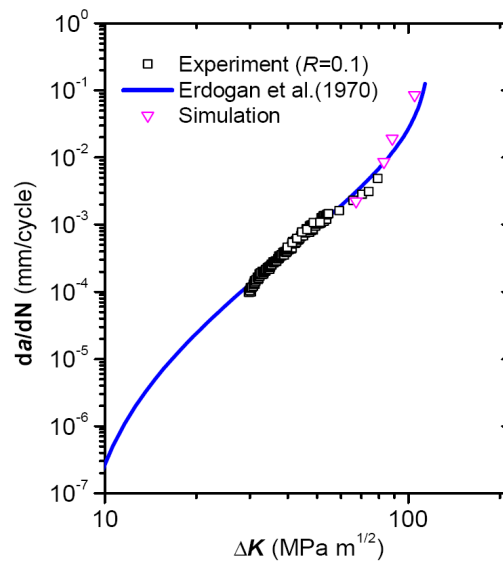


Figure 10. Comparison between the numerical simulation and the experimental data.

## 5. Concluding remarks

In the present paper a cohesive zone model in conjunction with monotonic damage and cyclic fatigue damage was investigated based on experimental tests, to create a unified fatigue crack growth model for both elastic and elastic-plastic fatigue crack growth.

In simulations the initial cohesive strength and the corresponding displacement jump are defined based on the true stress-strain relationship so that the cohesive zone does not affect the compliance of the specimen before damage initiation. The penetration of the crack surface under compression is prevented using the contact formulation. The first results confirm that the present cohesive zone model coupled with monotonic and cyclic damage evolution is suitable to describe fracture and fatigue crack growth of stainless steel 304 with severe plastic deformations.

In addition, the present computations reveal that the damage evolution in the low stress level and the material compression process could not be properly described need further improvement. More extensive studies on the cohesive model and the damage evolution equation may provide further understanding of ductile fatigue damage under more complex loading conditions.

### Acknowledgements

The authors thank financial support of the German Science Foundation (DFG) under the contact number YU119/8-1.

### References

- [1] Ortiz M., Pandolfi A., Finite-deformation irreversible cohesive elements for three-dimensional crack-propagation analysis. *International Journal for Numerical Methods in Engineering*, 44 (1999) 1267-82.
- [2] Xu Y., Yuan H., Computational modeling of mixed-mode fatigue crack growth using extended finite element methods. *International Journal of Fracture*, 159 (2009) 151-65.
- [3] Xu Y., Yuan H., Computational analysis of mixed-mode fatigue crack growth in quasi-brittle materials using extended finite element methods. *Engineering Fracture Mechanics*, 76 (2009) 165-81.
- [4] Wells G.N., Sluys L.J., A new method for modelling cohesive cracks using finite elements. *International Journal for Numerical Methods in Engineering*, 50 (2001) 2667-82.
- [5] de Borst R., Numerical aspects of cohesive-zone models. *Engineering Fracture Mechanics*, 70 (2003) 1743-57.
- [6] Freed Y., Banks-Sills L., A new cohesive zone model for mixed mode interface fracture in bimetals. *Engineering Fracture Mechanics*, 75 (2008) 4583-93.
- [7] Krull H., Yuan H., Suggestions to the cohesive traction–separation law from atomistic simulations. *Engineering Fracture Mechanics*, 78 (2011) 525-33.
- [8] Dugdale D.S., Yielding of steel sheets containing slits. *Journal of the Mechanics and Physics of Solids*, 8 (1960) 100-4.
- [9] Barenblatt G.I., The Mathematical Theory of Equilibrium Cracks in Brittle Fracture, in: H.L. Dryden T.v.K.G.K.F.H.v.d.D., Howarth L. (Eds.), *Advances in Applied Mechanics*, Elsevier, 1962, pp. 55-129.
- [10] Xu X.P., Needleman A., Numerical simulations of fast crack growth in brittle solids. *Journal of the Mechanics and Physics of Solids*, 42 (1994) 1397-434.
- [11] Yuan H., Lin G., Cornec A., Verification of a Cohesive Zone Model for Ductile Fracture. *Journal of Engineering Materials and Technology*, 118 (1996) 192-200.
- [12] Cornec A., Scheider I., Schwalbe K.-H., On the practical application of the cohesive model. *Engineering Fracture Mechanics*, 70 (2003) 1963-87.
- [13] Scheider I., Schödel M., Brocks W., Schönfeld W., Crack propagation analyses with CTOA and cohesive model: Comparison and experimental validation. *Engineering Fracture Mechanics*, 73 (2006) 252-63.
- [14] Yang B., Mall S., Ravi-Chandar K., A cohesive zone model for fatigue crack growth in quasibrittle materials. *International Journal of Solids and Structures*, 38 (2001) 3927-44.
- [15] Roe K.L., Siegmund T., An irreversible cohesive zone model for interface fatigue crack growth simulation. *Engineering Fracture Mechanics*, 70 (2003) 209-32.
- [16] Xu Y., Yuan H., On damage accumulations in the cyclic cohesive zone model for XFEM analysis of mixed-mode fatigue crack growth. *Computational Materials Science*, 46 (2009) 579-85.
- [17] Ural A., Krishnan V.R., Papoulia K.D., A cohesive zone model for fatigue crack growth allowing for crack retardation. *International Journal of Solids and Structures*, 46 (2009) 2453-62.
- [18] ABAQUS Version 6.10, ABAQUS Inc., Pawtucket, U.S.A., 2010.
- [19] Erdogan F., Ratwani M., Fatigue and fracture of cylindrical shells containing a circumferential crack. *Int J Fract*, 6 (1970) 379-92.